Available online at www.sciencedirect.com
SCIENCE DIRECT®
Journal of Magnetic Resonance 162 (2003) 443–453
JMR Journal of Magnetic Resonance
www.elsevier.com/locate/jmr

Enhanced triple-quantum excitation in ^{13}C magic-angle spinning NMR

Marina Carravetta,[a,b] Jörn Schmedt auf der Günne,[a,c] and Malcolm H. Levitt[b,*]

[a] *Physical Chemistry Division, Stockholm University, S-106 91, Sweden*
[b] *Chemistry Department, Southampton University, Southampton S017 1BJ, UK*
[c] *Institut für Anorganische Chemie, Universität Bonn, Germany*

Received 7 November 2002; revised 6 February 2003

Abstract

We describe a new method for exciting triple-quantum coherences in ^{13}C-labelled powder samples under MAS. The proposed method combines selective double-quantum excitation with rotational resonance and frequency-selective composite pulses. The spin dynamics of this new method are described theoretically. Numerical calculations of the spin dynamics are compared to experimental results on fully ^{13}C-labelled L-alanine. The observed triple-quantum filtering efficiency is around 10% for the most intense spectral peak. The method is also demonstrated on other fully ^{13}C-labelled compounds, including a uniformly ^{13}C-labelled amino acid.

1. Introduction

The correlated nuclear spin states known as multiple-quantum coherences are widely used in solid-state NMR for studying molecular motions [1–3], molecular geometry [4–17], and estimating the number of neighboring spins in clusters [18–24]. Many of these methods require the excitation of high multiple-quantum orders (larger than 2). However, in the case of coupled spins 1/2 in solids, high-order multiple-quantum excitation is often inefficient. This is especially the case when magic-angle spinning is performed in order to enhance resolution and sensitivity, as it is often necessary for demanding applications, for example structural investigation of many biological systems. Since magic-angle spinning (MAS) averages out the dipolar couplings, which are necessary for multiple-quantum excitation in spin 1/2 systems, dipolar recoupling methods [25–31] must be used, and it is difficult to control the spin dynamics with sufficient accuracy to allow high-order multiple-quantum excitation with reasonable efficiency.

In the case of nuclei such as ^{13}C, multiple-quantum excitation is especially difficult because of the large chemical shift interactions and the small size of the homonuclear dipolar couplings. High-order multiple-quantum ^{13}C coherences have been observed in static solids [21,22]. In [32], a broadband double-quantum (DQ) recoupling method was applied under MAS conditions on a single-quantum state to lead to triple-quantum coherence in $^{13}C_3$ systems under MAS, but the maximum experimental triple-quantum (TQ)-filtering efficiency for the total magnetization was only 4%. Recently, ^{13}C multiple-quantum (MQ) coherences up to order 10 were observed under fast MAS using zero-quantum recoupling techniques [23]. The experimental TQ efficiency of this technique is about 3%. A new TQ excitation method was demonstrated with enhanced efficiencies for coupled ^{1}H systems, but no ^{13}C results were shown [33].

In this paper, we apply a new approach to improve the excitation of triple-quantum coherences (TQC) under MAS. The method is applicable to clusters of three coupled spin 1/2 nuclei, in which one of the three nuclei has a well separated isotropic chemical shift from the other two. This is a common case in the ^{13}C NMR of labelled amino acids and peptides, where the carbonyl ^{13}C has an isotropic chemical shift value very different from those of the C^{α} and side chain aliphatic carbon atoms. We achieve an experimental TQ-filtering efficiency of 9% for the total three-spin magnetization.

* Corresponding author. Fax: +44-23-8059-3781.
E-mail address: mhl@soton.ac.uk (M.H. Levitt).

1090-7807/03/$ - see front matter © 2003 Elsevier Science (USA). All rights reserved.
doi:10.1016/S1090-7807(03)00059-4

The topology of the coupling network and the proposed excitation scheme is depicted in Fig. 1a. The three spins in each cluster are depicted by circles and the largest spin–spin couplings by lines. To a first approximation, the distant coupling between spins 1 and 3 is ignored. It is assumed that the separation between the isotropic chemical shifts of spins 1 and 2 is much larger than that between spins 2 and 3, i.e., $|\Delta\omega_{12}^{\mathrm{iso}}| \gg |\Delta\omega_{23}^{\mathrm{iso}}|$, where $\Delta\omega_{jk}^{\mathrm{iso}} = \omega_j^{\mathrm{iso}} - \omega_k^{\mathrm{iso}}$, and $\omega_j^{\mathrm{iso}} = -\gamma B_0(\delta_j^{\mathrm{iso}} - \delta^{\mathrm{ref}})$. Here δ_j^{iso} is the isotropic chemical shift of spin j and δ^{ref} is the chemical shift value corresponding to the reference frequency of the spectrometer. The experiment is carried out at rotational resonance [34–36] between spins 1 and 2, i.e., $\omega_r = |\Delta\omega_{12}^{\mathrm{iso}}|$, where $\omega_r/2\pi$ is the MAS spinning frequency in Hertz.

The pulse sequence involves the following steps: (A) selectively excite DQ coherences between spins 2 and 3, starting from a state of longitudinal magnetization; (B) create a three spin correlated state exploiting free evolution under rotational resonance between spins 1 and 2; (C) apply a frequency-selective radio-frequency (rf) pulse to spin 2 in order to create TQC. The intended evolution of the density operator components are sketched in Fig. 1b. In step A, the longitudinal sum magnetization of spins 2 and 3 is converted by the DQ recoupling sequence into a superposition of (±2)-quantum coherences. Spin 1 is not involved at this stage. In step B, rotational resonance is used to selectively recouple spins 1 and 2, leading to transfer of the DQ coherence between spins 1 and 3, antiphase with respect to spin 2 (depicted by operator components of the form $I_1^{\pm}I_{2z}I_3^{\pm}$). In step C, the state of spin 2 is manipulated selectively, without modifying the states of spins 1 and 3. This allows the creation of TQ operator components ($I_1^{\pm}I_2^{\pm}I_3^{\pm}$).

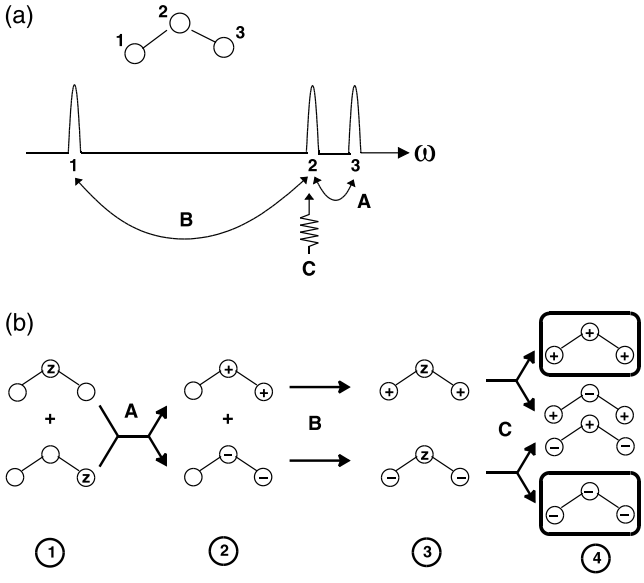

Fig. 1. (a) The model spin system and the atom numbering, together with the corresponding spectrum. The double-arrowed lines mark the recoupling modes active during the different pulse sequence blocks. Block **C** involves selective manipulation of spin S_2. (b) Graphical representation of the density operator transformations during the TQ excitation sequence.

As discussed below, the limiting efficiency of this process in powder samples for the total magnetization is around 21.5%. This represents a twofold enhancement in theoretical efficiency over the method discussed in [32]. In practice, there are losses due to relaxation and we achieve a TQ-filtering efficiency for the total magnetization of 8.7% on [U-^{13}C]-L-alanine, which is two times larger than the previously reported figure [32]. These enhancements improve the applicability of a variety of methods, such as spin counting schemes [24] and TQ-heteronuclear local field spectroscopy [12].

2. Materials and methods

The main model system used in this investigation is 98% [U-^{13}C]-L-alanine (Cambridge Isotope Laboratories), with the molecular structure shown in Fig. 2, together with the assignment of the spins S_1, S_2, and S_3. The internuclear distances for L-alanine are $r_{12} = 153.1$, $r_{23} = 152.4$, and $r_{13} = 251.8$ pm; the bond angle is $\theta = 111°$ [37]. The isotropic chemical shift differences are $|\Delta\delta_{12}^{\mathrm{iso}}| = 126.7$ and $|\Delta\delta_{23}^{\mathrm{iso}}| = 30.9$ ppm. In a field of 9.4 T the $n = 1$ rotational resonance [36] between S_1 and S_2 is observed at a spinning frequency of 12.750 kHz. All spin interaction parameters are known from previous studies [38]. All simulations were performed on three-spin 1/2 systems neglecting protons using either SIMPSON [39] or homebuilt software utilizing the COMPUTE algorithm [40].

All experiments on [U-^{13}C]-L-alanine were performed on a Varian Infinity Plus spectrometer operating at a field of 9.4 T on a full 3.2 mm rotor, using a decoupling field of $|\omega_{\mathrm{nut}}^{I}/2\pi| = 120$ kHz, if not otherwise stated. TPPM decoupling [41] was used during the acquisition and rotational resonance evolution periods. The TPPM sequence used pulses of duration 4.15 μs with phase shifts ±15°.

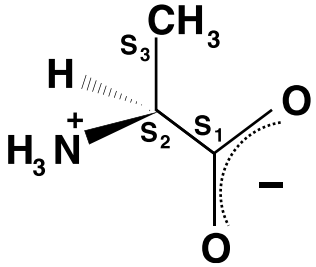

Fig. 2. Geometry of [U-^{13}C]-L-alanine.

Sodium 99%-[U-^{13}C]-propanoate and 98%-[U-^{13}C], 96%-[U-^{15}N]-L-histidine (both from Cambridge Isotope Laboratories) were studied at a field of 9.4 T, using full 4 mm rotors, with a proton decoupling field of $|\omega^I_{\rm nut}/2\pi| = 100$ kHz.

3. Triple-quantum pulse sequence

3.1. Structure

The pulse sequence for TQ coherence excitation is shown in Fig. 3. It is suitable for TQ excitation on powdered samples containing clusters of at least three-spin 1/2 nuclei with resolved isotropic chemical shifts. The channel marked *I* in Fig. 3 indicates irradiation at the frequency of the abundant spin species, in this case protons, ^{1}H. The channel marked *S* indicates irradiation at the frequency of the dilute spin species, here ^{13}C.

The pulse sequence consists of 8 blocks, denoted **P**, $\mathbf{A}_1$, $\mathbf{B}_1$, $\mathbf{C}_1$, $\mathbf{C}_2$, $\mathbf{B}_2$, $\mathbf{A}_2$, and **R**. The preparation block **P** consists of ramped cross-polarization [42] followed by a $\pi/2$ pulse with a $\pi/2$ phase shift, to prepare enhanced longitudinal *S*-magnetization. The blocks $\mathbf{A}_1$, $\mathbf{B}_1$, $\mathbf{C}_1$ convert this longitudinal magnetization into TQ coherence, as discussed in detail below. The blocks $\mathbf{C}_2$, $\mathbf{B}_2$, $\mathbf{A}_2$ reconvert the TQ coherence into longitudinal magnetization, which is transformed into observable transverse magnetization by the read pulse **R**. In the 2D experiment (see below), blocks $\mathbf{C}_1$ and $\mathbf{C}_2$ are separated by a variable evolution interval t_1 (not shown in Fig. 3) with CW proton decoupling.

The spectrometer reference frequency is different for each pulse sequence block and is denoted $\omega^P_{\rm ref}$, $\omega^A_{\rm ref}$, $\omega^B_{\rm ref}$, $\omega^C_{\rm ref}$, and $\omega^R_{\rm ref}$ in the discussion below. The spectrometer reference frequency during the evolution interval t_1 is denoted $\omega^E_{\rm ref}$. All frequency jumps are performed phase coherently [43].

The overall rf phases of the blocks are defined ϕ_P, ϕ_{A_1}, ϕ_{B_1}, ϕ_{C_1}, ϕ_{C_2}, ϕ_{B_2}, ϕ_{A_2}, and ϕ_R. The phase cycle selects the pathway corresponding to coherence order changes from 0 to ± 3 between block **P** to $\mathbf{C}_1$ and then 0 to -1 in block **R**. The 24-step phase cycle can be written as

$$\begin{aligned}
&\phi_P = \phi_{A_1} = \phi_{B_1} = \phi_{C_1} = \frac{2\pi k_2}{6} + \frac{\pi}{6}k_1 + \frac{2}{3}\omega_r t_1,\\
&\phi_{A_2} = \phi_{B_2} = \phi_{C_2} = 0,\\
&\phi_R = \frac{\pi}{2}\,\mathrm{floor}\left(\frac{k_2}{6}\right),\\
&\phi_{\rm rec} = 0,\\
&\phi_{\rm dig} = k_2\pi + \frac{\pi}{2}\,\mathrm{floor}\left(\frac{k_2}{6}\right),
\end{aligned} \tag{1}$$

where k_2 is the transient counter, $k_2 = 0, \ldots, 23$, k_1 is the transient counter in the indirect dimension for 2D experiments ($t_1 = k_1 = 0$ for one-dimensional experiments) and the function floor(x) returns the largest integer not greater than x, as defined in [44]. Here $\phi_{\rm rec}$ and $\phi_{\rm dig}$ are the reference phase during signal detection and the post-digitization phase shift, respectively. All phases take into account the rf mixing scheme and the sign of the gyromagnetic ratio [45,46]. The dependence of the phases $\phi_P = \phi_{A_1} = \phi_{B_1} = \phi_{C_1}$ on t_1 takes into account the time-

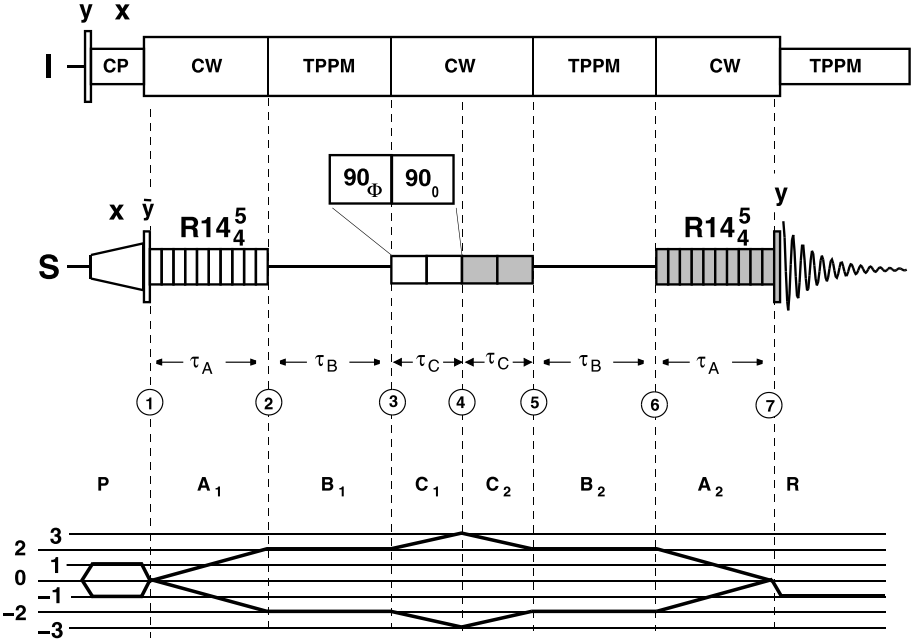

Fig. 3. Pulse sequence for TQC excitation and coherence transfer pathway diagram. The circled numbers represent time points.

proportional phase incrementation (TPPI) scheme for pure 2D spectroscopy [47] and the phase-time relationship of the γ-encoded recoupling schemes (see below).

3.2. Preparation

The pulse sequence starts with ramped cross-polarization [42] from the I spins to the S spins, followed by a $\pi/2$ pulse on the S spins to generate enhanced z-magnetization. The phases of the S-spin cross-polarization field and the $\pi/2$ pulse are ϕ_P and $\phi_P - \pi/2$, respectively.

A ^{13}C CP-MAS spectrum of [U-^{13}C]-L-alanine at a field of 9.4 T and a spinning frequency of $\omega_r/2\pi = 12.750$ kHz is shown in Fig. 4a. The cross-polarization contact time was 0.6 ms, the spectrometer reference frequency was set to $\omega^P_{\mathrm{ref}} = (\omega^{\mathrm{iso}}_1 + \omega^{\mathrm{iso}}_3)/2$, and the decoupling field during acquisition was set to $|\omega^I_{\mathrm{nut}}/2\pi| = 100$ kHz. The prominent splitting of the S_1 and S_2 resonances is due to rotational resonance [36] since the spinning frequency closely matches the isotropic chemical shift difference at this field. The small peak at the center of S_1 (carboxylate) is due to imperfect proton decoupling of the protonated S_2 (α-carbon) site [48].

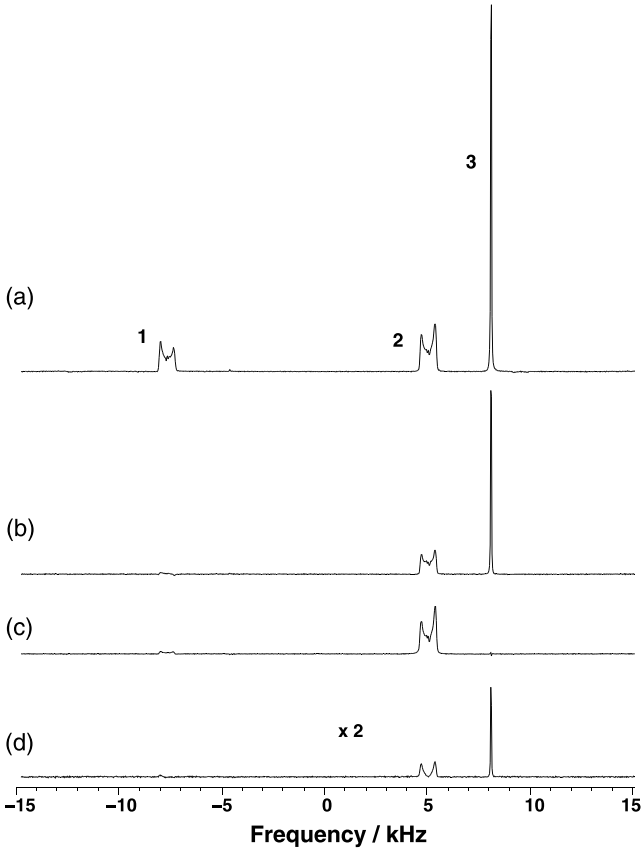

Fig. 4. Experimental spectra for 98%-[U-^{13}C]-L-alanine at 9.4 T with a spinning frequency of $\omega_r/2\pi = 12.750$ kHz, all acquired on a full 3.2 mm rotor under the same conditions and with 24 transients: (a) ramped CP spectrum with 0.6 ms contact time, the peak assignments are indicated; (b) DQ-filtered spectrum using $\mathrm{R}14^5_4$, with an rf field strength corresponding to $|\omega^S_{\mathrm{nut}}/2\pi| = 22.3$ kHz and a reference frequency of $\omega^{\mathrm{ref}}_A = (\omega^{\mathrm{iso}}_2 + \omega^{\mathrm{iso}}_2)/2$; (c) selective excitation of transverse magnetization using $90_0 90_{-80}$ and a reference frequency $\omega^{\mathrm{ref}}_C = \omega^{\mathrm{iso}}_2$; (d) TQF spectrum obtained using the sequence in Fig. 3, plotted with twice the vertical scale.

The time point at the end of the preparation block is denoted as ① in Fig. 3. The state of the spin ensemble at time point ① may be written as

$$\rho_{①} = S_{1z} + S_{2z} + S_{3z} \tag{2}$$

ignoring unnecessary factors, where S_{jz} is the z angular momentum operator for spin j. Since the operator S_{1z} is not exploited for the DQ excitation, it will now be omitted

$$\rho_{①} = S_{2z} + S_{3z}. \tag{3}$$

This state corresponds to the left-hand diagram in the cartoon of Fig. 1b.

3.3. Excitation of double-quantum coherence (step A)

Block $\mathbf{A}_1$ of the pulse sequence consists of a recoupling sequence for converting sum longitudinal magnetization of spins 2 and 3 into DQ coherence between spins 2 and 3. A pulse sequence of the form $\mathrm{R}14^5_4$ from the $\mathrm{R}N^v_n$-sequence family [28,30,31] with the basic element $\mathrm{R}^0 = 180_0$ was found to be suitable. This consists of a sequence of 180° pulses with alternating phase $\pm 5\pi/14$ rad (64.29°) and with 14 180° pulses occupying four rotor periods. The sequence uses rather low rf amplitudes. The nutation frequency of the rf field is $\omega^S_{\mathrm{nut}} = 1.75\omega_r$. In the present case, the nutation frequency was $|\omega^S_{\mathrm{nut}}/2\pi| = 22.3$ kHz.

Fig. 5 shows simulations of the three-spin DQ-filtering efficiency of two different $\mathrm{R}14^5_4$ sequences as a function of the carrier frequency ω^{ref}_A using parameters corresponding to the three-spin system of [U-^{13}C]-L-alanine at a field of 9.4 T. The three-spin DQ-filtering efficiency is defined as the fraction of the total z-magnetization in the three-spin 1/2 system that is converted into DQ coherence and back again. In the present case, since only two of the three-spins are exploited, the maximum theoretical efficiency in a powder is expected to be around $73\% \times 2/3 = 48.7\%$. As can be seen in Fig. 5, the $\mathrm{R}14^5_4$ sequence using the basic element $\mathrm{R}^0 = 180_0$ provides narrowband DQ recoupling, with a maximum efficiency close to the theoretical optimum. The $\mathrm{R}14^5_4$ sequence with the basic element $\mathrm{R}^0 = 90_0\ 270_{180}$ is much more broadband and actually achieves more efficiency than the 48.7% limit since it involves all three spins in the cluster. In the present case, the narrow bandwidth of the $\mathrm{R}14^5_4$ sequence with $\mathrm{R}^0 = 180_0$ is exploited by setting the spectrometer frequency to $\omega^{\mathrm{ref}}_A = (\omega^{\mathrm{iso}}_2 + \omega^{\mathrm{iso}}_3)/2$, so as to recouple spins 2 and 3 without recoupling spin 1 to the other two. The rf phases of the block $\mathbf{A}_1$ of the sequence in Fig. 3 were therefore $\phi_{A_1} \pm 5\pi/14$.

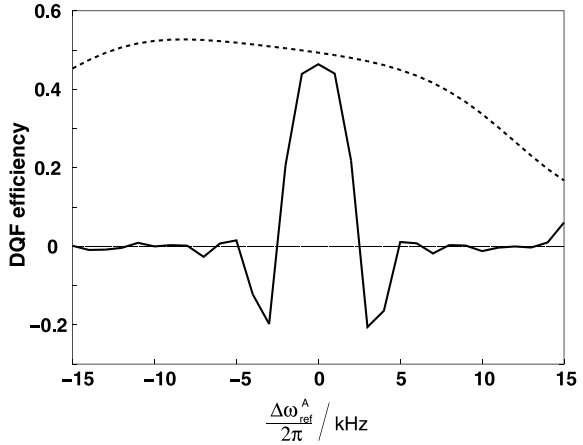

Fig. 5. Simulations of the DQ-filtering efficiency for the three-spin 1/2 system of [U-^{13}C]-L-alanine for $R14^5_4$ with $R^0 = 90_0270_{180}$ (dashed line) and with $R^0 = 180_0$. The abscissa is the carrier frequency offset $\Delta\omega^A_{ref} = \omega^A_{ref} - (\omega^{iso}_2 + \omega^{iso}_3)/2$. The spinning frequency is set to $\omega_r/2\pi = 12.750$ kHz and the field is 9.4 T. The simulation parameters are given in [37,38]. The composite pulse 90_0270_{180} provides broadband dipolar recoupling, which in not desirable in this experiment. The narrowband element $R^0 = 180_0$ recouples spins 2 and 3 selectively.

The effective Hamiltonian under the selective recoupling sequence is

$$\bar{\mathcal{H}}_A \approx \frac{1}{2}\left(\omega_A S_2^+ S_3^+ + \omega_A^* S_2^- S_3^-\right), \tag{4}$$

where the effective recoupling field ω_A depends upon the orientational angles and the dipolar coupling constant as follows:

$$\omega_A = \kappa_{2\text{–}122} b_{23} D^2_{0-1}(\Omega_{MR}) d^2_{-10}(\beta_{RL}) \times \exp\{i(\alpha^0_{RL} - \omega_r t_{①})\}, \tag{5}$$

where $b_{23}/2\pi = -(\mu_0/4\pi)\gamma^2\hbar/r^3_{23}$. The orientation of the molecule with respect to the rotor frame is described by the Euler angles $\Omega_{MR} = \{\alpha_{MR}, \beta_{MR}, \gamma_{MR}\}$. These three angles are random variables in a powder sample. The initial rotor position is denoted by the angle α^0_{RL} and $t_{①}$ is the starting time point of the sequence. $\kappa_{2\text{–}122}$ is the scaling factor of the recoupled term $\{l, m, \lambda, \mu\} = \{2, -1, 2, 2\}$, as described in [27]. The scaling factor for the other recoupled term is $\kappa_{212\text{–}2}$ and has the same magnitude. For the simple basic element $R^0 = 180_0$, the scaling factor is $|\kappa_{2\text{–}122}| = 0.16$, which is similar to that found for many other recoupling sequences [15,31].

In the following discussion, the double-quantum recoupling amplitude is written

$$\omega_A = |\omega_A| e^{i\phi_A}, \tag{6}$$

where the DQ recoupling phase has the following dependence on the orientational angle γ_{MR}:

$$\phi_A(\gamma_{MR}) = \phi^0_A + \gamma_{MR}. \tag{7}$$

This "γ-encoding" property follows from the selection of $\{l, m, \lambda, \mu\} = \{2, -1, 2, 2\}$ and $\{2, 1, 2, -2\}$ space-spin components by the $R14^5_4$ recoupling sequence [28,31].

Since the selective recoupling sequence may be assumed to isolate spins 2 and 3 dynamically from spin 1, the spin density operator at time point ② may be calculated through

$$\rho_{②} \approx \exp\{-i\bar{\mathcal{H}}_A\tau_A\}(S_{2z} + S_{3z})\exp\{i\bar{\mathcal{H}}_A\tau_A\} + \cdots \tag{8}$$

which leads to

$$\rho_{②} \approx (S_{2z} + S_{3z})\cos|\omega_A\tau_A| + S_2^+ S_3^+ i\, e^{i\phi_A}\sin|\omega_A\tau_A| - S_2^- S_3^- i e^{-i\phi_A}\sin|\omega_A\tau_A| \cdots. \tag{9}$$

The DQ operators correspond to the second frame in the cartoon of Fig. 1b. In the following, only the (±2)-quantum components of $\rho_{②}$ are retained.

Fig. 4b shows an experimental DQ-filtered spectrum of [U-^{13}C]-L-alanine using $R14^5_4$ at a spinning frequency of $\omega_r/2\pi = 12.750$ kHz and excitation/reconversion interval of duration $\tau_{A_1} = \tau_{A_2} = 627\,\mu$s. The DQ-filtering efficiency is 39% of the total three-spin 1/2 magnetization. Note the suppression of the S_1 resonance, which is beyond the bandwidth of the selective recoupling pulse sequence.

3.4. Rotational resonance evolution (step B)

The entire pulse sequence is conducted under $n = 1$ rotational resonance [36,48] between spins 1 and 2, i.e., the spinning frequency is chosen such that $\omega_r = |\omega^{iso}_1 - \omega^{iso}_2|$. The rotational resonance splittings are easily visible in the CP-MAS spectrum in Fig. 4a.

The theory in [36] may be used to estimate the rotational resonance evolution of the spin system. Since the rotational resonance recoupling is highly selective, the propagation operator for the spin system over the interval τ_B may be written as follows:

$$U_B \approx U^0_B(t_{③})\exp\{-i\bar{\mathcal{H}}_B\tau_B\}U^0_B(t_{②}), \tag{10}$$

where the recoupled zero-quantum Hamiltonian during the rotational resonance block **B** is

$$\bar{\mathcal{H}}_B \approx \frac{1}{2}\left(\omega_B S_1^+ S_2^- + \omega_B^* S_1^- S_2^+\right) \tag{11}$$

and

$$\omega_B = -b_{12} D^2_{0-1}(\Omega_{MR}) d^2_{-10}(\beta_{RL}) \exp\{i(\alpha^0_{RL} - \omega_r t_{②})\} \tag{12}$$

with $b_{12}/2\pi = -(\mu_0/4\pi)\gamma^2\hbar/r^3_{12}$. The zero-quantum recoupling amplitude may be written as

$$\omega_B = |\omega_B| e^{i\phi_B}, \tag{13}$$

where

$$\phi_B(\gamma_{MR}) = \phi^0_B + \gamma_{MR}. \tag{14}$$

This γ-dependence is the same as for ω_A (see Eq. (7)). This is because the $R14^5_4$ recoupling sequence and rotational resonance both recouple the $m = 1$ spatial component. This spatial compatibility of the two methods is essential for good TQ efficiency in a powder sample.

The propagator U_B^0 in Eq. (10) may be written as

$$U_B^0(t) \approx \exp\{-\mathrm{i}(\omega_1^{\mathrm{iso}} S_{1z} + \omega_2^{\mathrm{iso}} S_{2z} + \omega_3^{\mathrm{iso}} S_{3z})t\} \tag{15}$$

neglecting CSA terms. In general, this propagator gives rise to a phase shift of the excited TQ coherences, which must be taken into account by an opposite phase shift in the rf pulses. For simplicity, the effect of these propagators will be ignored in the following discussion.

The evolution of double-quantum coherence under the zero-quantum recoupled Hamiltonian of Eq. (11) may be estimated by using the following spin 1/2 commutation relationships:

$$\left[S_1^+ S_2^- \mathrm{e}^{\mathrm{i}\phi} + S_1^- S_2^+ \mathrm{e}^{-\mathrm{i}\phi}, S_1^\alpha S_2^+ S_3^+\right] = \mathrm{i}\,\mathrm{e}^{\mathrm{i}\phi} S_1^+ S_2^\alpha S_3^+, \tag{16}$$

$$\left[S_1^+ S_2^- \mathrm{e}^{\mathrm{i}\phi} + S_1^- S_2^+ \mathrm{e}^{-\mathrm{i}\phi}, S_1^+ S_2^\alpha S_3^+\right] = -\mathrm{i}\,\mathrm{e}^{\mathrm{i}\phi} S_1^+ S_2^\alpha S_3^+, \tag{17}$$

$$\left[S_1^+ S_2^- \mathrm{e}^{\mathrm{i}\phi} + S_1^- S_2^+ \mathrm{e}^{-\mathrm{i}\phi}, S_1^\beta S_2^+ S_3^+\right] = -\mathrm{i}\,\mathrm{e}^{\mathrm{i}\phi} S_1^+ S_2^\beta S_3^+, \tag{18}$$

$$\left[S_1^+ S_2^- \mathrm{e}^{\mathrm{i}\phi} + S_1^- S_2^+ \mathrm{e}^{-\mathrm{i}\phi}, S_1^+ S_2^\beta S_3^+\right] = \mathrm{i}\mathrm{e}^{\mathrm{i}\phi} S_1^+ S_2^\beta S_3^+, \tag{19}$$

where $S_j^\alpha = (1/2)\mathbb{I} + S_{jz}$ and $S_j^\beta = (1/2)\mathbb{I} - S_{jz}$. These properties lead to [44]

$$\begin{aligned}
&\exp\{-\mathrm{i}\bar{\mathcal{H}}_B\tau_B\} S_1^\alpha S_2^+ S_3^+ \exp\{\mathrm{i}\bar{\mathcal{H}}_B\tau_B\} \\
&\quad = S_1^\alpha S_2^+ S_3^+ \cos|\omega_B\tau_B| + \mathrm{i}\,\mathrm{e}^{\mathrm{i}\phi_B} S_1^+ S_2^\alpha S_3^+ \sin|\omega_B\tau_B|, \\
&\exp\{-\mathrm{i}\bar{\mathcal{H}}_B\tau_B\} S_1^\beta S_2^+ S_3^+ \exp\{\mathrm{i}\bar{\mathcal{H}}_B\tau_B\} \\
&\quad = S_1^\beta S_2^+ S_3^+ \cos|\omega_B\tau_B| - \mathrm{i}\,\mathrm{e}^{\mathrm{i}\phi_B} S_1^+ S_2^\beta S_3^+ \sin|\omega_B\tau_B|
\end{aligned}$$

and hence

$$\begin{aligned}
\rho_{③} \approx &-2\mathrm{e}^{\mathrm{i}(\phi_A+\phi_B)} \sin|\omega_A\tau_A| \sin|\omega_B\tau_B| \\
&\times \left(S_1^+ S_{2z} S_3^+ + S_1^- S_{2z} S_3^-\right) + \cdots.
\end{aligned} \tag{20}$$

This equation shows that the DQ coherence between spins 2 and 3 is converted into DQ coherences between spins 1 and 3, antiphase with respect to 2, by the rotational resonance evolution.

This conversion is strongly orientation-dependent, since the recoupling frequencies ω_A and ω_B are orientation-dependent. However, since the same spatial component ($m = 1$) is recoupled in both cases $\mathbf{A}_1$ and $\mathbf{B}_1$, the γ_{MR}-dependence of the two recoupling intervals are compatible.

The interval τ_B is adjusted in order to optimize the transfer over a powder. Experimentally, the interval τ_B was constrained to be a half integer number of rotor periods. In the experiment described here, the rotational resonance interval was $\tau_B = 592\,\mu\mathrm{s}$. The spectrometer reference frequency during the rotational resonance evolution was set to $\omega_B^{\mathrm{ref}} = (\omega_1^{\mathrm{iso}} + \omega_3^{\mathrm{iso}})/2$.

3.5. Selective composite pulse (step C)

For excitation of TQ coherence we need an rf pulse sequence that gives an effective $\pi/2$ rotation on spin 2 while leaving the states of spins 1 and 3 unchanged. In practice, we found a composite pulse sequence of the form $90_\Phi\ 90_0$ to be suitable, if the rf field is adjusted to the condition $\omega_{\mathrm{nut}}^S = (1/4)\omega_r$, the phase shift is $\Phi = 90°$ and the spectrometer reference frequency during the sequence **C** is set to be on-resonance with spin S_2, i.e., $\omega_{\mathrm{ref}}^C = \omega_2^{\mathrm{iso}}$. The frequency-selective sequence $90_\Phi\ 90_0$ has a total duration of two rotor periods.

Fig. 6 shows simulations of the performance of the $90_{90}90_0$ sequence on a model single spin 1/2 system as a function of the isotropic chemical shift. The nutation frequency in the rf field is 3.188 kHz, corresponding to the condition $\omega_{\mathrm{nut}}^S = \frac{1}{4}\omega_r$ at a spinning frequency of $\omega_r/2\pi = 12.750\,\mathrm{kHz}$. The arrows correspond to the ^{13}C isotropic chemical shifts in L-alanine at 9.4 T, assuming

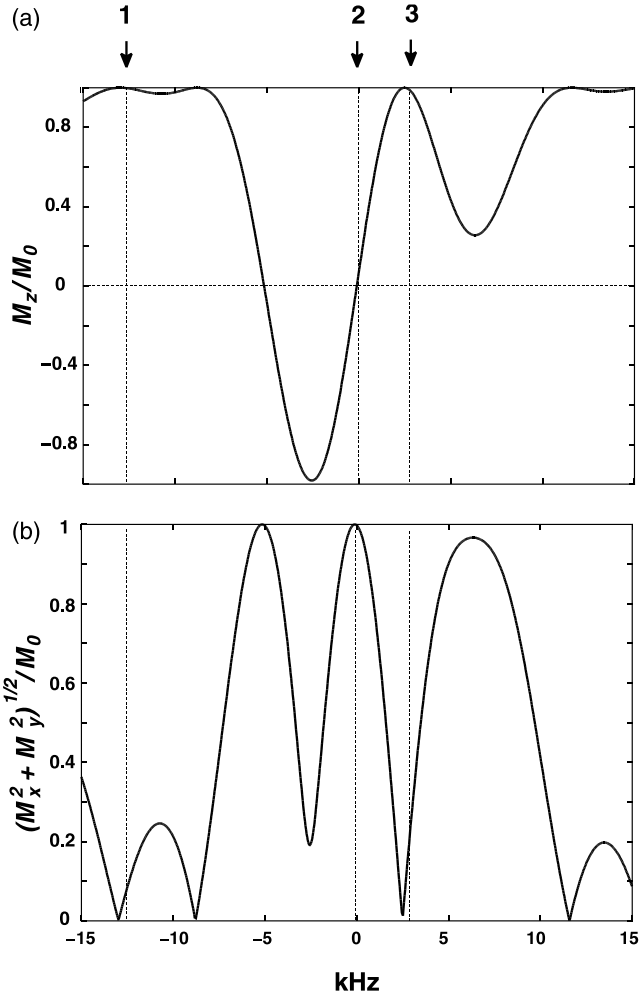

Fig. 6. Simulation of a $90_{90}90_0$ sequence on an isolated spin 1/2 ensemble. The rf field strength corresponds to $|\omega_{\mathrm{nut}}^S/2\pi| = 3.188$ kHz. The isotropic chemical shift positions of the three spins in [U-^{13}C]-L-alanine at 9.4 T are indicated by arrows. (a) Longitudinal magnetization M_z after the $90_{90}90_0$ sequence is applied to equilibrium magnetization. The magnetization M_z at position 2 is destroyed while the longitudinal magnetization at positions 1 and 3 are unperturbed. (b) Transverse magnetization $\sqrt{(M_x^2 + M_y^2)}/M_0$ after the $90_{90}90_0$ sequence is applied to equilibrium magnetization. Transverse magnetization is only excited on spin 2.

that the rf reference frequency is set to $\omega^C_{\rm ref} = \omega^{\rm iso}_2$. The initial state of the spin ensemble corresponds to pure longitudinal magnetization. The response of the spin ensemble is monitored as a function of the isotropic chemical shift difference, $\omega^0 - \omega^C_{\rm ref}$. When the isotropic shift frequency is on resonance ($\omega^0 = \omega^{\rm ref}_C$), corresponding to the arrow marked 2, the longitudinal magnetization is converted into transverse magnetization (i.e., $M_z/M_0 \approx 0$ in Fig. 6a and $\sqrt{M_x^2 + M_y^2}/M_0 \approx 1$ in Fig. 6b). In the regions corresponding to the isotropic shifts of spins S_1 and S_3 the magnetization stays along the z-axis ($M_z/M_0 \approx 1$ and $\sqrt{M_x^2 + M_y^2}/M_0 \approx 0$).

If the spin–spin couplings and the chemical shift anisotropies are ignored during the sequence C, the propagator for the three-spin system may be written as

$$U_C \approx R_1(\Omega^{(1)}_C) R_2(\Omega^{(2)}_C) R_3(\Omega^{(3)}_C), \tag{21}$$

where the Euler angles are written as $\Omega^{(j)}_C = \{\alpha^{(j)}_C, \beta^{(j)}_C, \gamma^{(j)}_C\}$, the rotation operators are $R_j(\Omega_j) = R_{jz}(\alpha^{(j)}_C) R_{jy}(\beta^{(j)}_C) R_{jz}(\gamma^{(j)}_C)$ with $R_{j\mu}(\theta) = \exp\{-{\rm i}\theta S_{j\mu}\}$. For the sequence $90_{90}90_0$, with an rf field corresponding to $|\omega^S_{\rm nut}/2\pi| = 3.188\,{\rm kHz}$, isotropic shift frequency $\omega^{\rm iso}_1/2\pi = -12.750$, $\omega^{\rm iso}_2/2\pi = 0$, and $\omega^{\rm iso}_1/2\pi = 3.083\,{\rm kHz}$, the three sets of Euler angles may be evaluated numerically to be $\Omega^{(1)}_C = \{124.3°, 4.1°, -145.7°\}$, $\Omega^{(2)}_C = \{180°, 90°, -90°\}$, and $\Omega^{(3)}_C = \{53.4°, 16.3°, 143.4°\}$. The transformation of antiphase DQ coherence may be written as

$$\begin{aligned} U_C S_1^+ S_{2z} S_3^+ U_C^\dagger = {} & \frac{1}{8}(1 + \cos\beta^{(1)}_C)(1 + \cos\beta^{(3)}_C) \\ & \times \sin\beta^{(2)}_C S_1^+ S_2^+ S_3^+ \times \exp\{-{\rm i}(\alpha^{(1)}_C \\ & + \gamma^{(1)}_C + \alpha^{(3)}_C + \gamma^{(3)}_C + \alpha^{(2)}_C)\} + \cdots. \end{aligned} \tag{22}$$

Since the phases in the complex exponential add up approximately to 360°and the angles $\beta^{(1)}_C$ and $\beta^{(3)}_C$ are small, the conversion into TQ is almost optimal.

In practice, the realistic three-spin system in [U-^{13}C]-L-alanine behaves slightly differently, due to spin–spin couplings and chemical shift anisotropy during the composite pulse. Experiments and simulations indicate slightly better performance with $\Phi \approx 80°$ for the case of alanine.

The practical performance of the $90_{80}90_0$ pulse sequence is illustrated by the spectrum in Fig. 4c. This spectrum was produced by applying the $90_{80}90_0$ sequence to longitudinal ^{13}C magnetization generated by ramped cross-polarization followed by a $90_{\bar y}$ ^{13}C pulse, 90° out of phase, as in block **P**, with phase cycling used to suppress single-quantum terms before the composite pulse. As may be seen, the selective excitation of transverse S_2 magnetization is very efficient and the suppression of S_1 and S_3 signals is almost ideal.

Fig. 6 shows that the response of the composite pulse is highly asymmetric with respect to the sign of the frequency offset. The correct operation of the composite pulse demands careful handling of the sign of the rf phase shifts. The recommendations in [45,46] must be followed rigorously.

3.6. Reconversion and observation

The TQ coherence is reconverted into observable transverse magnetization by repeating the steps **C**, **B**, **A** in inverse order, followed by the $\pi/2$ read pulse **R**.

In practice, the sequence $\mathbf{C}_2$ is given an overall −80° phase shift with respect to $\mathbf{C}_1$, in order to compensate the extra z-rotations $\phi^{(1)}_C$, $\phi^{(2)}_C$, and $\phi^{(3)}_C$ (Eq. (21)). The rf phases during the blocks $\mathbf{C}_1$ and $\mathbf{C}_2$ were therefore $\{\phi_{C_1} + \Phi, \phi_{C_1}\}$ and $\{\phi_{C_2}, \phi_{C_2} - \Phi\}$, where $\Phi = 80°$ and the phases ϕ_{C_1} and ϕ_{C_2} take part in the phase cycling procedure (Eq. (1)).

The reference frequency was set to $\omega^R_{\rm ref} = (\omega^{\rm iso}_1 + \omega^{\rm iso}_3)/2$ during the read 90° pulse and during signal detection.

3.7. Triple-quantum evolution (step E)

For two-dimensional experiments an interval of proton-decoupled free evolution is inserted between blocks $\mathbf{C}_1$ and $\mathbf{C}_2$. The triple-quantum coherences evolve at the sum of the isotropic chemical shifts, giving rise to a sharp triple-quantum peak, independent of the rotational resonance splitting in the single-quantum spectrum. However, the frequency of this peak must be calculated with care since the rotation of the sample during the t_1 interval modulates the recoupling Hamiltonians. This shifts the apparent frequency of the triple-quantum peak, independent of the coherent evolution occurring during the t_1 interval.

Consider the effective Hamiltonian for the reconversion block $\mathbf{B}_2$. According to Eqs. (11) and (12), the effective recoupling field depends upon the starting time point $t_⑤$ as

$$\omega_B(t_⑤) = \omega_B(0)\exp\{-{\rm i}\omega_r t_⑤\}. \tag{23}$$

The dependence of the propagator under the second rotational resonance period on the time point $t_⑤$ is conveniently expressed in terms of selective rotations of spin S_1 as

$$\bar{\mathcal{H}}_B(t_⑤) = R_{1z}(\omega_r t_⑤)\bar{\mathcal{H}}_B(0)R_{1z}(-\omega_r t_⑤), \tag{24}$$

where $R_{jz}(\beta) = \exp\{-{\rm i}\beta S_{jz}\}$. Similarly, Eqs. (4) and (6) allow the time-dependence of the propagator for the second recoupling sequence, $\mathbf{A}_2$, to be written as

$$\bar{\mathcal{H}}_A(t_⑥) = R_{3z}(\omega_r t_⑥)\bar{\mathcal{H}}_A(0)R_{3z}(-\omega_r t_⑥). \tag{25}$$

These expressions may be used to follow the fate of the coherence transfer pathways $S_1^\pm S_2^\pm S_3^\pm \to S_1^\pm S_{2z} S_3^\pm \to S_2^\pm S_3^\pm \to S_z$ leading to the final NMR signal. The right-

most rotation in Eq. (24) imposes a phase shift on the $S_1^{\pm}S_{2z}S_3^{\pm}$ terms according to

$$R_{1z}(-\omega_r t_{⑤})S_1^{\pm}S_{2z}S_3^{\pm}R_{1z}(\omega_r t_{⑤}) = S_1^{\pm}S_{2z}S_3^{\pm}\exp\{\mathrm{i}\omega_r t_{⑤}\}. \quad (26)$$

The leftmost rotation operator in Eq. (24) is selective for spin S_1 and does not affect the $S_2^{\pm}S_3^{\pm}$ terms. These coherences pick up another phase factor from the rightmost rotation in Eq. (25) according to

$$R_{3z}(-\omega_r t_{⑥})S_2^{\pm}S_3^{\pm}R_{3z}(\omega_r t_{⑥}) = S_2^{\pm}S_3^{\pm}\exp\{\mathrm{i}\omega_r t_{⑥}\}. \quad (27)$$

As the evolution interval t_1 is incremented, the time points $t_{⑤}$ and $t_{⑥}$ change synchronously, so the complex NMR signal acquires the factor $\exp\{\mathrm{i}2\omega_r\}$, which appears as a frequency shift of twice the spinning frequency.

In Eq. (1), this spurious frequency shift is eliminated by a phase shift of $2\omega_r t_1/3$ of the entire excitation block, $\{\mathbf{P}, \mathbf{A}_1, \mathbf{B}_1, \mathbf{C}_1\}$. The divisor of 3 is needed since the phase rotation acts on TQ coherence at time point $t_{④}$.

4. Overall efficiency

In a powder sample, the overall TQ-filtering efficiency for the total 3-spin magnetization, assuming ideal pulse sequence performance throughout, is given by

$$F_{3Q}(\tau_A, \tau_B) = \int_0^{\pi/2} \mathrm{d}\beta \sin^2(|\omega_A\tau_A|)\sin^2(|\omega_B\tau_B|) \times \sin\beta \times \frac{2}{3} \times \frac{1}{2}, \quad (28)$$

where ω_A and ω_B depend upon the Euler angle β according to Eqs. (6) and (12). The factor 2/3 arises because only 2 out of 3 spins are involved and the factor 1/2 arises from the generation of undesirable single-quantum terms at step **C** (see Fig. 1). The function $F_{3Q}(\tau_A, \tau_B)$ has a maximum value of 21.5%.

If the unitary bound [49] could be achieved simultaneously for all molecular orientations, the overall TQ-filtering efficiency would be 75%. The current experiment is therefore still a long way from the theoretical optimum.

In systems of spin 1/2 pairs, the maximum DQ efficiency in powder samples for γ-encoded DQ recoupling sequences [5] is 73%. It might be anticipated that the maximum efficiency for the current experiment would be $73\% \times 73\% \times \frac{2}{3} \times \frac{1}{2} \approx 18\%$, where one factor comes from the DQ recoupling step and one from the rotational resonance step. The theoretical efficiency is higher in practice because the orientation dependence of the two pulse sequence transformations are highly correlated. Those molecular orientations which give high efficiency in one step also give high efficiency in the second step.

5. Results

5.1. One-dimensional spectra

Fig. 4d shows a TQ-filtered spectrum of [U-^{13}C]-L-alanine obtained using the pulse sequence in Fig. 3 with TPPM decoupling ($|\omega_{\mathrm{nut}}^I/2\pi| = 120$ kHz in block **B** and **R**), using the phase cycling in Eq. (1) to suppress signals not passing through (±3Q)-coherences at time point ④ and with 8 s delay between acquired transients. The absence of peak 1 is due to the use of the selective DQ-sequence, as previously explained. The TQ-filtering efficiency is 8.7% of the total z magnetization, as estimated by comparing the integrated spectral intensity with respect to the corresponding CP spectrum. This compares favourably with the previous best reported figure of 4% [32]. The discrepancy between the maximum theoretical figure of 21.5% and the experimental figure of 9% is mainly due to relaxation losses.

In many experimental situations, the filtering efficiency for the total magnetization does not give an accurate representation of the loss of signal-to-noise suffered when performing multiple-quantum filtration, since the filtered magnetization is not distributed evenly on the filtered spectral peaks. The ratio of the amplitude of the most intense spectral peak in the filtered spectrum to the amplitude of the same peak in an unfiltered experiment is sometimes a more straightforward guide to practicability.

In Fig. 4d, the TQ-filtering efficiency for the narrow S_3 (CH_3) peaks is about 10%. This is higher than the filtering efficiency for the total magnetization, which is 8.7%, since the spectral amplitude is concentrated on the peaks of spins 2 and 3. Similarly, the method of Edén and Levitt [32] achieved a TQ-filtering efficiency of 4% for the total magnetization but 8% for the CH_2 peak, which acquires most of the TQ-filtered signal in that experiment. Note, however, that it is experimentally more favourable to gather signal on the CH_3 peak since this site is the terminal point of the coupled three-spin topology and generates much narrower NMR signals. As a result, the new method has advantages over that given in [32] even if the experimental filtering efficiency for the strongest peaks are nominally quite similar.

The efficiency is consistently better when using TPPM decoupling during blocks $\mathbf{B}_1$ and $\mathbf{B}_2$ and signal acquisition (as shown in Fig. 3), rather then CW. Further improvements may be anticipated using improved heteronuclear decoupling technology [50,51], especially in conjunction with small diameter rotors, allowing higher decoupling fields.

The efficiency may be compared with the recently described methods of Oyler and Tycko [23]. The plotted simulations indicate that at most 6% of the total magnetization recovered at the end of the pulse sequence passes through TQC in the case of fully labelled amino

acids. The experimental efficiencies is lower since not all of the initial magnetization is recovered into observable signal and because of relaxation losses, which are typically at least 50%. The TQ-filtering efficiency of the Oyler and Tycko method is 2.6% on a sample of [U-^{13}C]-L-valine [52], compared with the cross-polarization signal.

The performance of the pulse sequence on other spin systems was also verified. Fig. 7 shows the experimental ramped-CP and TQ-filtered spectra on a sample of sodium [U-^{13}C]-propanoate, acquired with 4 and 24 transients, respectively, using a delay between transients of 30 s. The spinning frequency was $\omega_r/2\pi = 15.540$ kHz corresponding to the $n = 1$ rotational resonance condition. The TQ-filtered spectrum was acquired using $\tau_A = 514\,\mu s$, $\tau_B = 483\,\mu s$, $\Phi = 105°$, $|\omega^I_{nut}/2\pi| = 100$ kHz, and $\phi_{TPPM} = \pm 10°$ and gives a TQF efficiency of 7.5% for the narrow S_3 peak.

Fig. 8 shows the experimental ramped-CP and TQ-filtered spectra for [U-^{13}C]-L-histidine, acquired with 4 and 24 transients, respectively, using a delay between transients of 15 s, $\tau_A = 620\,\mu s$, $\tau_B = 626\,\mu s$, $\Phi = 87°$, spinning frequency $\omega_r/2\pi = 11.979$ kHz, $|\omega^I_{nut}/2\pi| =$ 100 kHz, and $\phi_{TPPM} = \pm 34°$ in block **B**. The TQF efficiency for the narrow C^β peak was 8.0%.

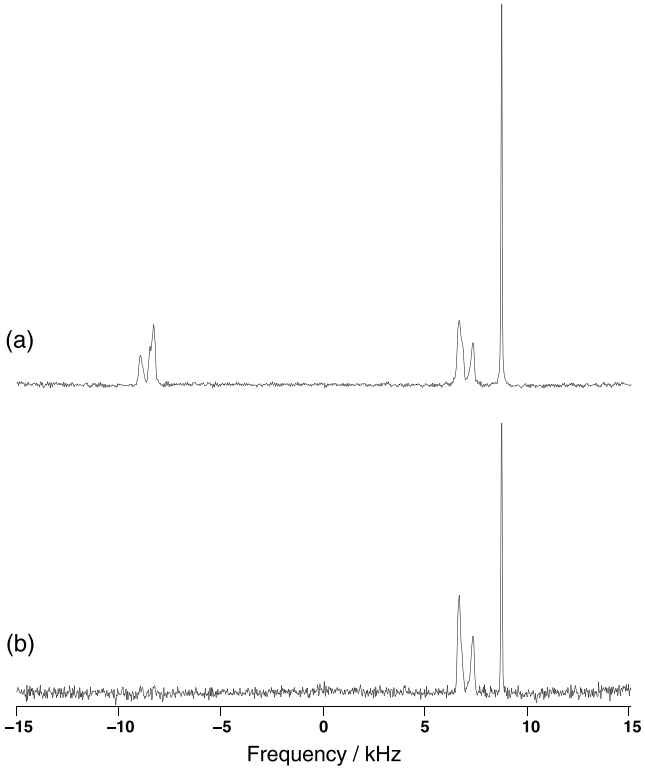

Fig. 7. (a) Ramped CP spectrum of sodium [U-^{13}C]propanoate at 9.4 T, $\omega_r/2\pi = 15.540$ kHz, 4 transients, acquired with a recycle delay of 30 s and TPPM decoupling, using $|\omega^I_{nut}/2\pi| = 100$ kHz and $\phi_{TPPM} = \pm 10°$; (b) triple-quantum filtered spectrum, acquired in 24 transients using $\tau_A = 514\,\mu s$, $\tau_B = 483\,\mu s$, $\Phi = 105°$, $|\omega^I_{nut}/2\pi| = 100$ kHz, and $\phi_{TPPM} = \pm 10°$. The TQ-filtering efficiency for the S_3 peak is 7.9% (5.4% with respect to the total three-spin magnetization).

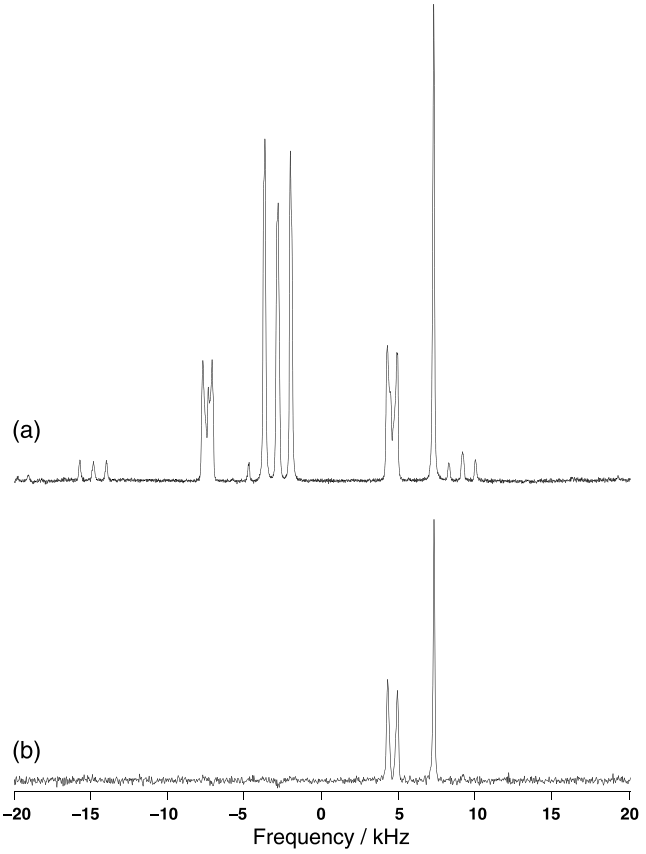

Fig. 8. (a) Ramped CP spectrum of [U-^{13}C]-L-histidine at 9.4 T, $\omega_r/2\pi = 11.979$ kHz, 4 transients, acquired with a pulse delay of 15 s and TPPM decoupling using $|\omega^I_{nut}/2\pi| = 100$ kHz and $\phi_{TPPM} = \pm 13°$; (b) triple-quantum filtered spectrum, acquired in 24 transients using $\tau_A = 620\,\mu s$, $\tau_B = 626\,\mu s$, $\Phi = 87°$, $|\omega^I_{nut}/2\pi| = 100$ kHz, and $\phi_{TPPM} = \pm 34°$ in block **B**. The TQ-filtering efficiency for the C^β peak is 8.0%.

This shows that this TQ excitation strategy is not limited to isolated spin systems and should even be feasible on uniformly labelled proteins. The slightly lower efficiency for these two samples may be due to the lower decoupling fields available on 4 mm probes and to inhomogeneity effects related to the larger sample volumes used in these cases.

5.2. Two-dimensional spectrum

The precession frequency of the triple-quantum coherences may be measured by acquiring a data matrix $s(t_1, t_2)$ using variable evolution t_1 interval between the blocks $\mathbf{C}_1$ and $\mathbf{C}_2$, followed by a two-dimensional Fourier transform. Fig. 9 shows a 2D spectrum recorded at 9.4 T on 98%-[U-^{13}C]-L-alanine using 1024 t_1 increments spaced by 25 μs and a delay between transients of 6 s. The pulse sequence parameters were $\tau_A = 627\,\mu s$, $\tau_B = 588\,\mu s$, $\omega^E_{ref} \approx (\omega^{iso}_1 + \omega^{iso}_3)/2$. The phase cycle

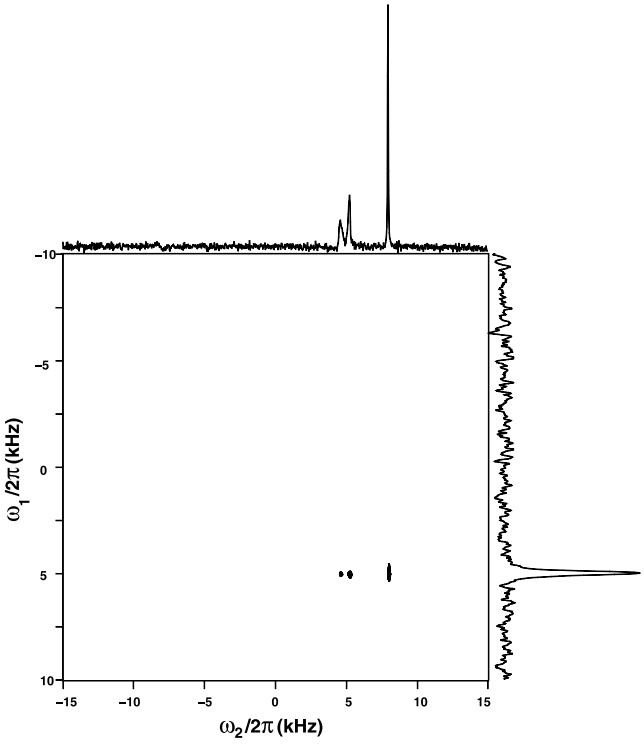

Fig. 9. 2D triple-quantum spectrum of [U-^{13}C]-L-alanine, obtained by the pulse sequence in Fig. 3, using continuous wave decoupling with $|\omega^I_{\rm nut}/2\pi| = 120$ kHz throughout and with an evolution interval t_1 inserted between blocks $\mathbf{C}_1$ and $\mathbf{C}_2$. The t_1 interval was incremented in 1024 steps of 25 μs, 6 transients each, with $\tau_A = 627$ μs, $\tau_B = 588$ μs, $\omega^{2D}_{\rm ref} = \omega^B_{\rm ref}$, and 6 s delay between transients. The phase cycle is given in Eq. (1). The total experimental time was 10 h 15 min.

described in Section 3.1 was used, including the time-proportional phase shift $2\omega_r t_1/3$ discussed above. The acquired data matrix was processed according to the TPPI scheme [47].

As can be seen, the indirect dimension contains a unique TQ peak about 400 Hz wide. The frequency of this peak is $\omega_{TQ}/2\pi = 5.007$ kHz, which corresponds closely to the estimated sum of the isotropic chemical shift frequencies $(\omega^{\rm iso}_1 + \omega^{\rm iso}_2 + \omega^{\rm iso}_3 - 3\omega^E_{\rm ref})/2\pi = 5.043$ kHz. The small discrepancy may be due to the difficulty of measuring isotropic chemical shifts in coupled spin systems. There is no evidence of any other TQ coherences deriving from intermolecular contacts.

6. Conclusions

We have demonstrated a new rf pulse sequence which leads to enhanced triple-quantum excitation for the magic-angle spinning NMR of certain ^{13}C-labelled systems, especially amino acids and proteins. The enhancement in efficiency will assist the application of pulse sequences exploiting high-order multiple-quantum coherences, such as spin counting experiments [24] and torsion angle determination [12].

In particular, TQ-NCCN torsion angle measurements [12] become greatly enhanced by the use of this method. The absence of the CO peak and the splitting of the C^α peak are not a serious disadvantage, since the information is transmitted to the narrow, intense C^β peak.

Despite these enhancements, triple-quantum coherences are still associated with considerable loss in NMR signal. Nevertheless, the spin counting work on amyloid fibrils [22] shows that such experiments are feasible on systems with a reasonable high molecular mass, even in the absence of magic-angle spinning. The work described in this paper will facilitate studies of this type and should be regarded as a step on the way to efficient high-order multiple-quantum experiments in solid-state NMR, which would have wide applications.

Acknowledgments

This research was supported by the EPSRC (UK), by the Göran Gustafsson Foundation for Research in the Natural Sciences and Medicine and by the German Science Foundation (Grant SCHM1570-1/1). We thank Mattias Edén for a copy of Ref. [33] prior to publication.

References

[1] A. Wokaun, R.R. Ernst, Mol. Phys. 36 (1978) 317.
[2] J. Tang, A. Pines, J. Chem. Phys. 72 (1980) 3290–3297.
[3] S.P. Brown, H.W. Spiess, Chem. Rev. 101 (2001) 4125–4155.
[4] H. Geen, J.J. Titman, J. Gottwald, H.W. Spiess, Chem. Phys. Lett. 227 (1994) 79–86.
[5] Y.K. Lee, N.D. Kurur, M. Helmle, O.G. Johannessen, N.C. Nielsen, M.H. Levitt, Chem. Phys. Lett. 242 (3) (1995) 304–309.
[6] B.Q. Sun, P.R. Costa, D. Kocisko, R.T. Lansbury, R.G. Griffin, J. Chem. Phys. 102 (1995) 702–707.
[7] D.M. Gregory, M.A. Mehta, J.C. Shiels, G.P. Drobny, J. Chem. Phys. 107 (1997) 28–42.
[8] X. Feng, Y.K. Lee, D. Sandström, M. Edén, H. Maisel, A. Sebald, M.H. Levitt, Chem. Phys. Lett. 257 (1996) 314–320.
[9] P.R. Costa, J.D. Gross, M. Hong, R.G. Griffin, Chem. Phys. Lett. 280 (1997) 95–103.
[10] X. Feng, P.J.E. Verdegem, Y.K. Lee, D. Sandström, M. Edén, P. Bovee-Geurts, W.J. de Grip, J. Lugtenburg, H.J.M. de Groot, M.H. Levitt, J. Am. Chem. Soc. 119 (1997) 6853–6857.
[11] K. Nomura, K. Takegoshi, T. Terao, K. Uchida, M. Kainosho, J. Biomol. NMR 17 (2000) 111–123.
[12] M. Edén, A. Brinkmann, H. Luthman, L. Eriksson, M.H. Levitt, J. Magn. Reson. 144 (2000) 266–279.
[13] C.P. Jaroniec, B.A. Tounge, J. Herzfeld, R.G. Griffin, J. Am. Chem. Soc. 123 (2001) 3507–3519.
[14] V. Ladizhansky, M. Veshtort, R.G. Griffin, J. Magn. Reson. 154 (2002) 317.
[15] M. Carravetta, M. Edén, O.G. Johannessen, H. Luthman, P.J.E. Verdegem, J. Lugtenburg, A. Sebald, M.H. Levitt, J. Am. Chem. Soc. 123 (2001) 10628–10638.
[16] K. Saalwächter, H.W. Spiess, J. Chem. Phys. 114 (2001) 5707–5728.
[17] I. Schnell, H.W. Spiess, J. Magn. Reson. 151 (2001) 153–227.

[18] J. Baum, A. Pines, J. Am. Chem. Soc. 108 (1986) 7447–7454.
[19] D. Suter, S.B. Liu, J. Baum, A. Pines, Chem. Phys. 114 (1987) 103–109.
[20] H. Geen, R. Graf, A.S.D. Heindrichs, B.S. Hickman, I. Schnell, H.W. Spiess, J.J. Titman, J. Magn. Reson. 138 (1999) 167–172.
[21] O.N. Antzutkin, R. Tycko, J. Chem. Phys. 110 (1999) 2749–2752.
[22] O.N. Antzutkin, J.J. Balbach, R.D. Leapman, N.W. Rizzo, J. Reed, R. Tycko, Proc. Natl. Acad. Sci. 97 (2000) 13045–13050.
[23] N. Oyler, R. Tycko, J. Phys. Chem. B 106 (2002) 8382–8389.
[24] C.E. Hughes, J. Schmedt auf der Günne, M.H. Levitt, Phys. Chem., in press.
[25] A.E. Bennett, R.G. Griffin, S. Vega, NMR Basic Princ. Progr. 33 (1994) 1–77.
[26] M. Hohwy, H.J. Jakobsen, M. Edén, M.H. Levitt, N.C. Nielsen, J. Chem. Phys. 108 (7) (1998) 2686–2694.
[27] A. Brinkmann, M. Edén, M.H. Levitt, J. Chem. Phys. 112 (19) (2000) 8539–8554.
[28] M. Carravetta, M. Edén, A. Brinkmann, X. Zhao, M.H. Levitt, Chem. Phys. Lett. 321 (2000) 205–215.
[29] R. Tycko, G. Dabbagh, Chem. Phys. Lett. 173 (1990) 461.
[30] A. Brinkmann, M.H. Levitt, J. Chem. Phys. 115 (2001) 357–384.
[31] M.H. Levitt, Encyclopedia of Nuclear Magnetic Resonance: Supplementary Volume (2002) 165–196.
[32] M. Edén, M.H. Levitt, Chem. Phys. Lett. 293 (1998) 173–179.
[33] M. Edén, Chem. Phys. Lett. 366 (2002) 469–476.
[34] E.R. Andrew, A. Bradbury, R.G. Eades, V.T. Wynn, Phys. Lett. 4 (1963) 99–100.
[35] M.G. Colombo, B.H. Meier, R.R. Ernst, Chem. Phys. Lett. 146 (1988) 189–196.
[36] M.H. Levitt, D.P. Raleigh, F. Creuzet, R.G. Griffin, J. Chem. Phys. 92 (1990) 6347–6364.
[37] M.S. Lehmann, T.F. Koetzle, W.C. Hamilton, J. Am. Chem. Soc. 94 (1972) 2657–2660.
[38] A. Naito, S. Ganapathy, K. Akasaka, C.A. McDowell, J. Chem. Phys. 74 (1981) 3190–3197.
[39] M. Bak, J.T. Rasmussen, N.C. Nielsen, J. Magn. Reson. 147 (2000) 296–330.
[40] M. Edén, Y.K. Lee, M.H. Levitt, J. Magn. Reson. A 120 (1996) 56–71.
[41] A.E. Bennett, C.M. Rienstra, M. Auger, K.V. Lakshmi, R.G. Griffin, J. Chem. Phys. 103 (1998) 6951–6958.
[42] G. Metz, X. Wu, S.O. Smith, J. Magn. Reson. A 110 (1994) 219–227.
[43] A. Bielecki, A.C. Kolbert, H.J.M. de Groot, R.G. Griffin, M.H. Levitt, Adv. Magn. Res. 14 (1990) 111.
[44] M.H. Levitt, Spin Dynamics. Basics of Nuclear Magnetic Resonance, Wiley, New York, 2001.
[45] M.H. Levitt, J. Magn. Reson. 126 (1997) 164–182.
[46] M.H. Levitt, O.G. Johannessen, J. Magn. Reson. 142 (2000) 190–194.
[47] R.R. Ernst, G. Bodenhausen, A. Wokaun, Principles of Nuclear Magnetic Resonance in One and Two Dimensions, Clarendon Press, Oxford, 1988.
[48] M. Helmle, Y.K. Lee, P.J.E. Verdegem, X. Feng, T. Karlsson, J. Lugtenburg, H.J. de Groot, M.H. Levitt, J. Magn. Reson. 140 (1999) 379–403.
[49] O.W. Sørensen, J. Magn. Reson. 86 (1990) 435–440.
[50] P. Tekely, P. Palmas, D. Canet, J. Magn. Reson. A 107 (1994) 129–133.
[51] A. Detken, E.H. Hardy, M. Ernst, B.H. Meier, Chem. Phys. Lett. 356 (2002) 298–304.
[52] N. Oyler, R. Tycko, private communication.

Further reading

[1] S. Dusold, A. Sebald, Ann. Rep. NMR Spectrosc. 41 (2000) 185–264.